



Contents lists available at ScienceDirect

Bioorganic & Medicinal Chemistry Letters

journal homepage: www.elsevier.com/locate/bmcl

Structure-guided evolution of a 2-phenyl-4-carboxyquinoline chemotype into PPAR α selective agonists: New leads for oculo-vascular conditions

Xiao-Zheng Dou^{a,c}, Dinesh Nath^{a,c}, Younghwa Shin^b, Jian-Xing Ma^b, Adam S. Duerfeldt^{a,*}

^a Department of Chemistry & Biochemistry, Stephenson Life Sciences Research Center, University of Oklahoma, Norman, OK, United States

^b Department of Physiology, University of Oklahoma Health Sciences Center, Oklahoma City, OK, United States

ARTICLE INFO

Article history:

Received 2 February 2018

Revised 1 March 2018

Accepted 2 March 2018

Available online xxxxx

Keywords:

PPAR α

Age-related macular degeneration

Diabetic retinopathy

PPAR selectivity

Structure-based design

ABSTRACT

Small molecule agonism of PPAR α represents a promising new avenue for the development of non-invasive treatments for oculo-vascular diseases like diabetic retinopathy and age-related macular degeneration. Herein we report initial structure–activity relationships for the newly identified quinoline-based PPAR α agonist, Y-0452. Preliminary computational studies led to the hypothesis that carboxylic acid transposition and deconstruction of the Y-0452 quinoline system would enhance ligand–protein interactions and better complement the nature of the binding pocket. A focused subset of analogs was designed, synthesized, and assessed for PPAR α agonism. Two key observations arose from this work 1) contrary to other PPAR α agonists, incorporation of the fibrate “head-group” decreases PPAR α selectivity and instead provides *pan*-PPAR agonists and 2) computational models reveal a relatively unexploited amphiphilic pocket in PPAR α that provides new opportunities for the development of novel agonists. As an example, compound **10** exhibits more potent PPAR α agonism ($EC_{50} = \sim 6 \mu\text{M}$) than Y-0452 ($EC_{50} = \sim 50 \mu\text{M}$) and manifests >20-fold selectivity for PPAR α over the PPAR γ and PPAR δ isoforms. More detailed biochemical analysis of **10** confirms typical downstream responses of PPAR α agonism including PPAR α upregulation, induction of target genes, and inhibition of cell migration.

© 2018 Elsevier Ltd. All rights reserved.

Despite a number of treatment options (e.g., laser photocoagulation, blood-glucose regulation, corticosteroids and anti-vascular endothelial growth factor (VEGF) injections), the ability to address the complex nature of diabetic retinopathy (DR) and related oculo-vascular diseases (e.g., wet age-related macular degeneration) remains a significant challenge.^{1–3} Anti-VEGF has emerged as the primary treatment option, but suffers from the requirement of frequent intraocular injections, high cost, and the need for specialized facilities. Additionally, although effective for most, ~ 40 – 50% of patients are refractory to intravitreal injection of anti-VEGF and corticosteroids.^{3,4} This implies that auxiliary pathways and factors that remain unaddressed with current interventions are involved in disease causation and progression. A critical need exists to develop new treatment options that are non-invasive and complementary to current approaches.

Peroxisome proliferator-activated receptors (PPARs) are a family of nuclear hormone-activated receptors and transcription

factors that consists of three members, PPAR α , PPAR γ and PPAR δ .^{5,6} Although PPAR isoforms share significant sequence homologies, they exhibit diverse functions, have different tissue distributions, and can be selectively targeted.^{7–10} Within this family, PPAR α has garnered the most attention as a therapeutic target. PPAR α regulates the expression of genes involved in hyperlipidemia, diabetes, and inflammatory disorders and agonism of PPAR α provides pharmacological benefits for these conditions.^{10,11} Only recently, however, have the roles of PPAR α in regulating inflammation, apoptosis, and neovascularization (NV) in diabetic retinae been revealed, establishing a new avenue for PPAR α agonists as therapeutics for oculo-vascular diseases.^{12,13}

Two independent large clinical studies (FIELD and ACCORD) demonstrate that fenofibrate (Fig. 1), a widely used drug in the clinic for the treatment of hyperlipidemia, has robust protective effects against diabetic macular edema (DME) and retinal NV in type 2 diabetic patients.^{14,15} Fenofibrate represents the first orally available and safe drug with proven clinical efficacy on retinal NV and DME in humans with DR. This finding has excited clinicians, researchers and pharmaceutical companies who are interested in new drug treatments for oculo-vascular diseases. The protective

* Corresponding author.

E-mail address: adam.duerfeldt@ou.edu (A.S. Duerfeldt).

^c Authors contributed equally.

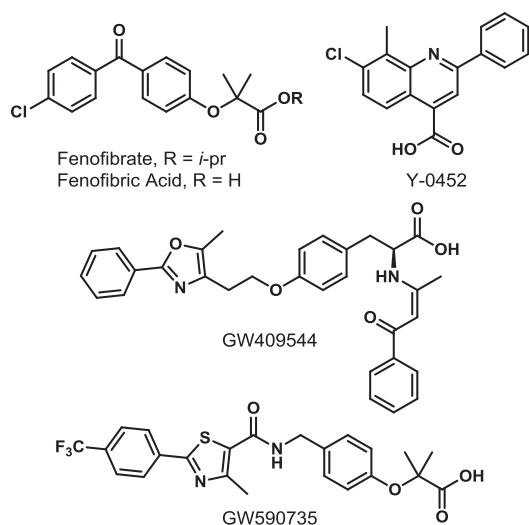


Fig. 1. PPAR α agonists referenced in this manuscript.

effects of fenofibrate on retinal NV and DME are unrelated to its lipid-lowering activity, but rather result from its agonism of PPAR α .^{12,16} To date, fenofibrate is the only PPAR α agonist known to cross the blood-ocular barrier and provide protective effects against DME and NV. Fenofibrate however, suffers from low ocular distribution, low affinity for PPAR α , lack of selectivity between PPAR isoforms, and dose-limiting toxicities, all of which will limit its use as a DR therapy.^{16–21} The clinical results paired with recent biochemical confirmation,^{12,22–24} however, demonstrate that small molecule PPAR α agonists with improved potency and enhanced ocular distribution have high promise to become non-invasive treatment options for oculo-vascular conditions.

Recently, a new PPAR α agonist, 7-chloro-8-methyl-2-phenylquinoline-4-carboxylic acid (Y-0452, Fig. 1), was reported.²³ Y-0452 displays protective effects *in vivo* against DR and exhibits anti-inflammatory, anti-angiogenic and neuroprotective effects without signs of toxicity in the retinas of mice and diabetic rats.²³ Y-0452 is structurally distinct from fenofibrate, making it an attractive lead; however, Y-0452 exhibits only weak on-target activity in biochemical PPAR α assays ($EC_{50} \approx 25\text{--}50 \mu\text{M}$), and manifests a low level of agonism compared to known PPAR α agonists.²³ Additionally, the highly-functionalized quinoline core of Y-0452 represents significant synthetic challenges regarding comprehensive structure-activity relationship (SAR) studies. These aspects inspired us to investigate the SAR of Y-0452 through molecular simplification with a goal of enhancing synthetic tractability, target engagement, selectivity, and level of PPAR α agonism. Towards this initiative, we utilized structure-based approaches to design a series of derivatives, which were then synthesized and evaluated for PPAR α agonism. The results from these studies are reported herein.

To gain insight into the potential binding modes of Y-0452 to PPAR α , we conducted docking studies with the Schrödinger Drug Discovery Suite. For these initial computational studies we selected PDB 1K7L, a co-crystal structure of GW409544 (Fig. 1) bound to human PPAR α (hPPAR α).²⁵ Although GW409544 exhibits 10-fold higher selectivity for hPPAR γ ($EC_{50} = 0.28 \text{ nM}$) over hPPAR α ($EC_{50} = 2.3 \text{ nM}$)²⁵ this structure was selected on the basis that detailed structural analyses of this chemotype and its interactions with different hPPAR isoforms are available for comparison and the data have been well-validated in subsequent studies.²⁵

To validate our docking approach, constraints, and parameters, GW409544 was extracted, exposed to MM2 energy-minimization, and re-docked into the hPPAR α ligand binding domain to ensure

that the results reproduced the bound conformation of the ligand. As shown in Fig. 2A, the overlay of co-crystallized (cyan) and docked (orange) GW409544 shows excellent congruence (RMSD = 0.34 Å). Maintaining the same constraints and parameters, Y-0452 was docked into hPPAR α and the results were analyzed for strategies to improve or introduce key interactions. Previous studies have demonstrated the significance of hydrogen bond interactions between hPPAR α Ser280, Tyr314, His440, and Tyr464 and the carboxylate motif of ligands.^{18,25–31} Interactions with all four of these residues is believed to be responsible for triggering full agonism of hPPAR α .²⁷ Poorer agonists tend to only interact with some of these hydrogen-bonding partners. As can be seen in Fig. 2B, while the quinoline core of Y-0452 provides a π -system for additional beneficial ligand-protein interactions via edge-to-face stacking with His440, the position of the carboxylate group on Y-0452 is predicted to only allow for two of the four possible hydrogen bonds (Tyr464 and His440).

We hypothesized that deconstruction of the quinoline core would 1) provide a more synthetically tractable scaffold amenable to facile assessment of carboxylate location and 2) relieve the rigidity encompassed within the aromatic 2-phenyl-carboxyquinoline chemotype. Although conformational constraint is a common technique used in medicinal chemistry to reduce entropic penalties through conformational bias, we hypothesized that, in this case, the rigidity of Y-0452 may be disadvantageous when the fragment is “grown” to fit the “U-shaped” binding pocket. We anticipated, however, that over simplification of an already modest hit may lead to inactive compounds, simply due to a reduction in surface area, thus limiting beneficial ligand-protein interactions. Indeed, simple *N*-benzylated variants of **1** (Fig. 2C) resulted in inactive derivatives (data not included). Docking of the simple *N*-benzylated analogs, however, revealed a 180° rotation of the molecules in the binding pocket, which positioned the substituted benzyl group in the same pocket as the oxazole of GW409544. Taking this into account and recognizing the value in the molecular orientation, we utilized structure-guided design to develop **9–14** and **21–24** that filled the hydrophobic binding pocket more efficiently. This focused set of analogs allowed us to test our hypothesis that quinoline deconstruction and transposition of the carboxylic acid would provide improved PPAR α agonists.

Derivatives **9–14** were synthesized as shown in Scheme 1. Commercially available 4-hydroxybenzaldehyde was coupled with various benzyl bromides **3–8** to afford benzaldehydes **3a–8a**. Treatment of **3a–8a** with 3-aminobenzoic acid produced the respective imines *in situ*, which were then reduced upon the addition of sodium triacetoxyborohydride to provide **9–14** in an unoptimized 40–82% yield.

In addition to the benzoic acid derivatives **9–14**, we wanted to incorporate the classical fibrate “head-group” with an aim to improve potency and instill selectivity for PPAR α over other isoforms.³¹ The preparation of these analogs is depicted in Scheme 2. Commercially available 3-nitrophenol was coupled with ethyl α -bromoisobutyrate to afford **15**, which was then reduced to the corresponding aniline (**16**) under catalytic hydrogenation conditions (H_2 and Pd/C in ethanol). Treatment of **16** with **3a**, **4a**, **6a**, or **8a** followed by reduction with sodium triacetoxyborohydride yielded **17–20**, respectively. Hydrolysis of the pendant ester gave the desired products **21–24** in an unoptimized 46–88% yield.

With the focused subset of Y-0452 analogs in-hand, our efforts shifted to the evaluation of these derivatives for PPAR α agonism. Preliminary evaluation utilized a commercially available PPAR α luciferase cell reporter assay (Indigo Biosciences). The cell-line employed is engineered to constitutively express high-levels of hPPAR α . Upon interaction with an agonist, hPPAR α translocates to the nucleus, binds to the PPAR response element (PPRE), and upregulates gene transcription, including the inserted luciferase

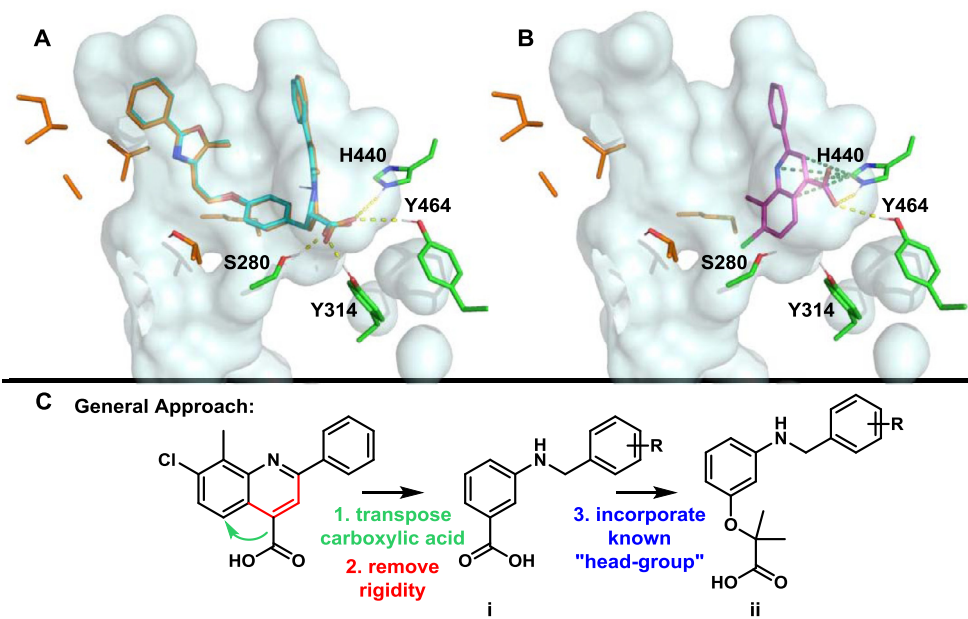
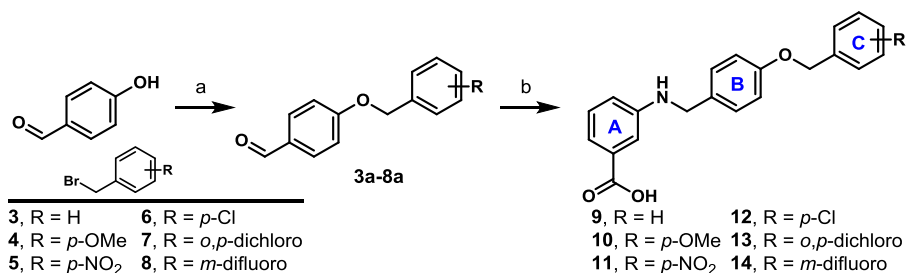
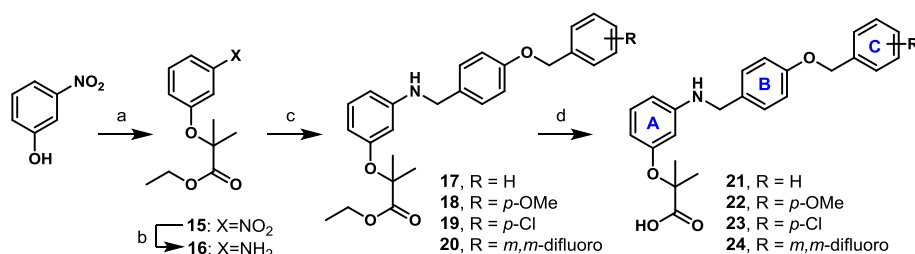


Fig. 2. A) Overlay of GW409544 extract (cyan) with GW409544 docked (orange). B) Y-0452 docked. Binding pocket cavity depicted by pale cyan surface, PDB: 1K7L. C) Molecular deconstruction approach for Y-0452 to provide the targeted analogs.



Scheme 1. Synthesis of benzoic acid derivatives **9–14**. Reagents and conditions: (a) benzyl bromide (i.e., **3–8**), K_2CO_3 , DMF, $80^\circ C$, 12 h; (b) 3-aminobenzoic acid, toluene, $155^\circ C$, 2 h; sodium triacetoxyborohydride, AcOH, THF, $0^\circ C$ to $25^\circ C$, 12 h.



Scheme 2. Synthesis of **21–24**. Reagents and conditions: (a) ethyl α -bromoisobutyrate, K_2CO_3 , DMF, $80^\circ C$, 12 h; (b) H_2 , Pd/C, ethanol, 12 h; (c) aldehyde (i.e., **3a**, **4a**, **6a**, or **8a**), toluene, $155^\circ C$, 2 h; sodium triacetoxyborohydride, AcOH, THF, $0^\circ C$ to $25^\circ C$, 12 h; (d) LiOH-H₂O, THF/MeOH/H₂O, 12 h.

gene. Luciferase activity is detected indirectly through quantification of oxyluciferin production. Initially, **9–14** and **21–24** were evaluated at $5\ \mu M$ and $50\ \mu M$ to provide an idea of agonism-level at two 10-fold increments. As shown in Fig. 3, a number of compounds exhibited levels of hPPAR α agonism on par with or surpassing the positive control, GW590735 ($5\ \mu M$ and $10\ \mu M$), at one or both of the concentrations evaluated. Direct comparison of **9/21**, **10/22**, **12/23**, **14/24** reveals that incorporation of the fenofibrate “head-group” enhances the level of PPAR α agonism at $50\ \mu M$. This data also indicates, however, that incorporation of the fibrate “head-group” decreases potency, as **21–24** fail to elicit

appreciable activity at $5\ \mu M$, whereas the benzoic acid analogs **9–14** all exhibit significant PPAR α agonism at this lower concentration. Compounds **10** and **22** were selected for more detailed evaluation, and a more expansive 10-point dose-response assessment was conducted to obtain EC₅₀ values (Table 1): **10** ($5.6\ \mu M$), and **22** ($25.3\ \mu M$).

To further confirm that this 4-benzyloxy-benzylamino chemotype acts as a PPAR α agonist, we evaluated compound **10** in various biochemical assays. As expected for a PPAR α agonist, **10** induced the expression of PPAR α in a dose-dependent manner (Fig. 4A and B), as demonstrated by Western blot analysis using a

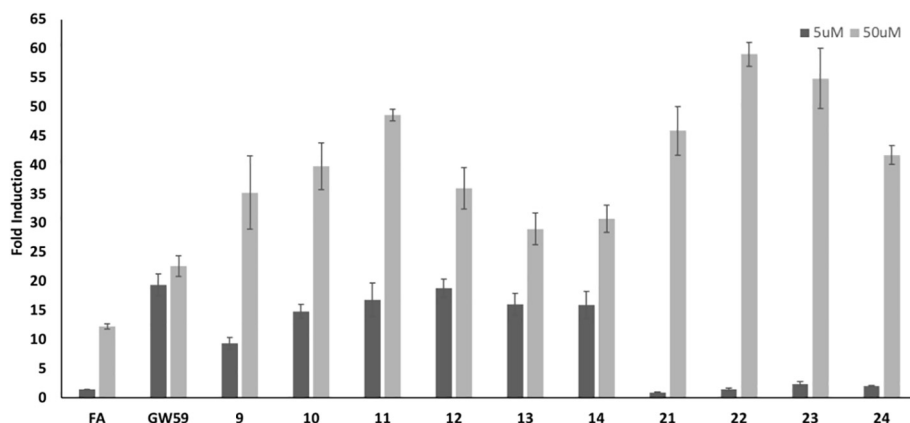


Fig. 3. Initial evaluation results of **9–14** and **21–24** for hPPAR α agonism. Results presented from a single experiment as fold-induction versus the DMSO control \pm S.E. ($n = 3$). GW590735 was evaluated at 5 and 10 μ M due to observed cytotoxicity at higher concentrations.

Table 1

Human PPAR agonism of select analogs. Data are represented as the EC₅₀ (μ M) for the agonism of the corresponding luciferase reporter cell-lines (Indigo Biosciences). Dosing was done in triplicate as a single experiment. n.d. = not determined. Values in parentheses indicate the ratio of agonism compared to GW590735.

Compound	EC ₅₀ (μ M)		
	hPPAR α	hPPAR δ	hPPAR γ
10	5.6 (1.5)	>100	>100
22	25.3 (1.7)	38.6	18.3
26	5.1 (1.1)	>100	>100
28	2.1 (1.4)	8.9	5.6
GW590735	0.012	n.d.	n.d.
Rosiglitazone	n.d.	n.d.	0.083
GW0742	n.d.	0.002	n.d.
Y-0452	52.4 (0.3)	n.d.	n.d.

cell line derived from C57BL/6N mouse photoreceptors (661 W). Likewise, RT-PCR studies on the same cell-line confirm PPAR α agonism, as treatment with **10** induces the expression of various

PPAR α target genes (Fig. 4C),³² including acyl-CoA dehydrogenase medium chain (*Acadm*), carnitine palmitoyltransferase 1A (*Cpt1a*), fatty acid binding protein 3 (*Fabp3*), and solute carrier family 25 member 20 (*Slc25a20*). Compound **10** was also evaluated in an *in vitro* wound healing assay utilizing human retinal capillary endothelial cells (HRCEC). PPAR α agonism reduces cell migration¹² and **10**, indeed, inhibits wound closure in a dose-dependent fashion (Fig. 4D).

Convinced that 4-benzyloxy-benzylamino derivatives exhibit characteristic PPAR α agonistic activity in several biological settings, the selectivity of **10** for PPAR α agonism over PPAR δ and PPAR γ was assessed. Luciferase assays were conducted on isogenic cell-lines engineered to overexpress either PPAR δ or PPAR γ with expression of the requisite luciferase reporter gene dependent upon exogenous activation of each isoform. As shown in Table 1, compound **10** exhibits ≥ 20 -fold selectivity for hPPAR α over hPPAR δ and hPPAR γ , whereas **22** displays *pan*-agonism. This is interesting, as the fibrate “head-group” has been described as a

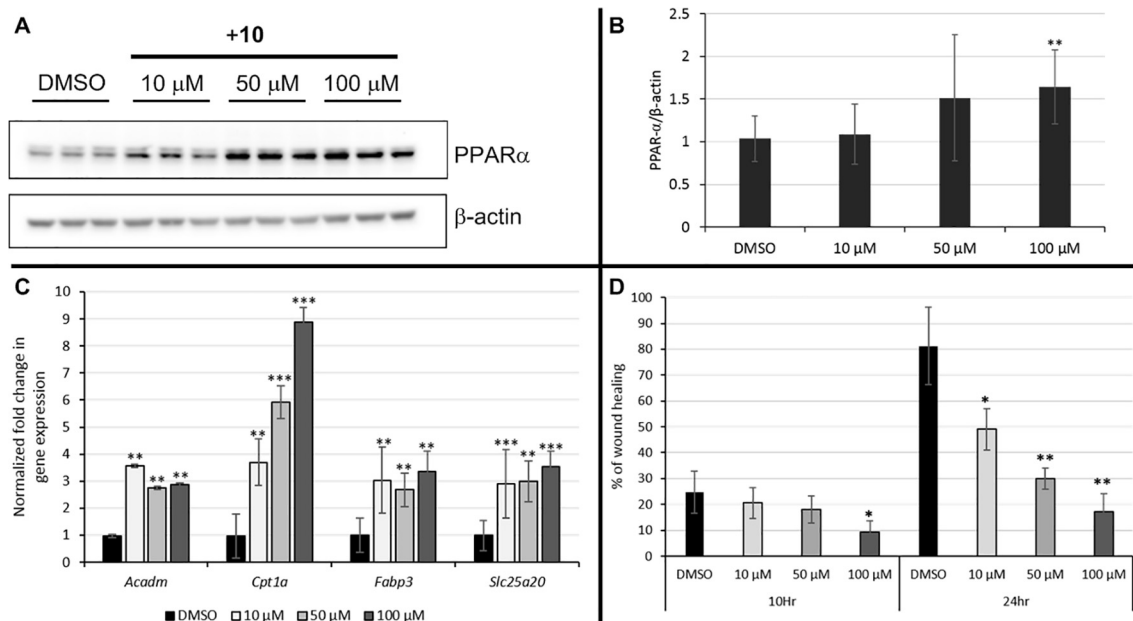


Fig. 4. Biochemical analysis of **10**. A) Western blot analysis of mouse 661 W cells after 24 h treatment with **10**. B) Densitometry quantification of PPAR α production from Western blot analysis. C) RT-PCR analysis of mouse 661 W cells after 24 h ($n = 6$) treatment with **10**. D) HRCEC wound healing assay results for both 10 h and 24 h incubation time points. Experiments were performed three times in triplicate unless otherwise noted. All values shown are expressed as mean \pm S.D. Differences between groups were tested for statistical significance using the Student's *t*-test. * $P < 0.05$, ** $P < 0.01$, *** $P < 0.001$.

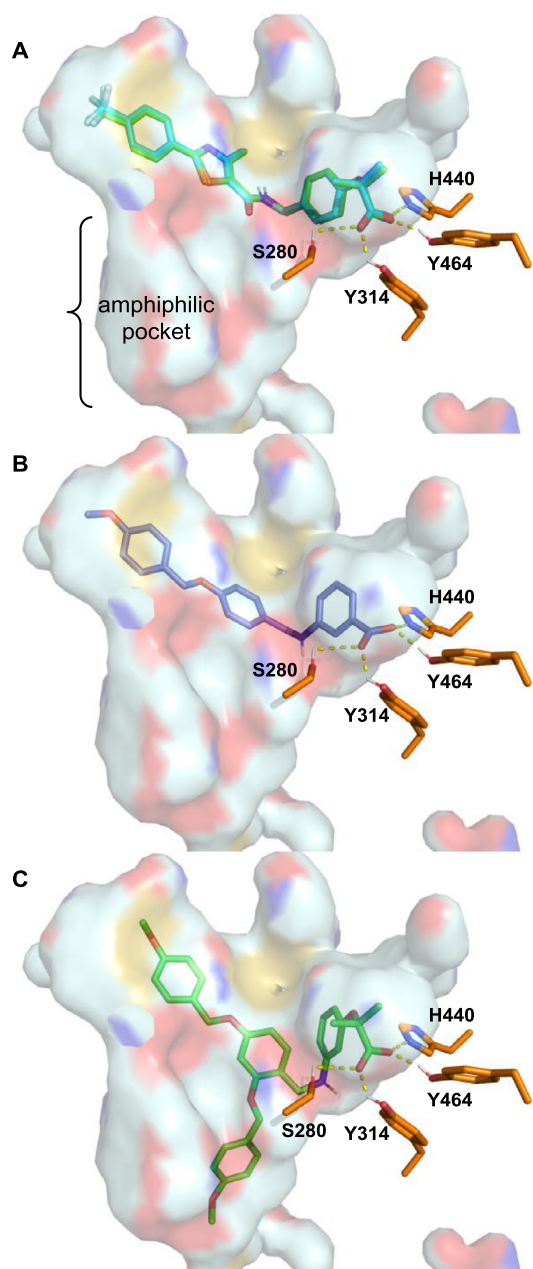


Fig. 5. A) Co-crystallized (green) and docked (cyan) GW590735. B) Predicted binding pose of **10**. C) Predicted binding pose of **28**. Binding pocket cavity depicted by surface representation, PDB: 2P54.

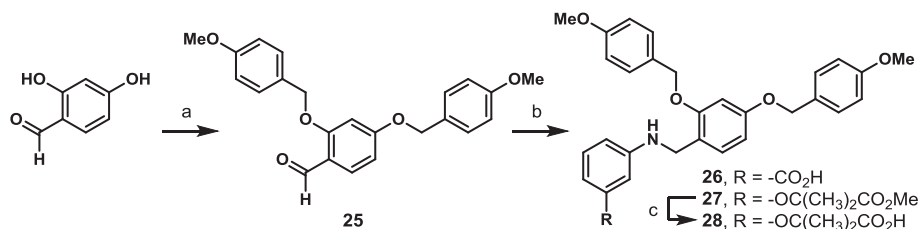
critical feature for PPAR α selectivity,¹⁰ but with this 4-benzyloxy-benzylamino chemotype it seems to be detrimental.

To better visualize the 4-benzyloxy-benzylamino derivatives in the hPPAR α binding pocket, we utilized PDB 2P54, the

GW590735-hPPAR α co-crystal structure, for docking assessment (see Supporting information). GW590735 is a selective PPAR α agonist that exhibits ≥ 500 -fold selectivity for PPAR α over PPAR γ and PPAR δ .³¹ As shown in Fig. 5A and B, compound **10** is predicted to bind in an orientation similar to GW590735. Interestingly, however, **10** lacks the gem-dimethyl “head-group” and amide linker domain, both of which have been postulated to be critical determinants in GW590735 selectivity and major enhancers of potency.³¹ The acid, however, for **10** is predicted to make four hydrogen bonds with Ser280, Tyr314, His440, and Tyr464, consistent with our hypothesis that deconstruction of the Y-0452 quinoline core and transposition of the carboxylic acid would provide a significant improvement in PPAR α agonism. We were interested if this 4-benzyloxy-benzylamino chemotype could be expanded to take advantage of an apparent amphiphilic pocket that lies below GW590735 (Fig. 5A) and is comprised of Met330, Tyr334, Glu282, Thr279, Met320, Val324, Leu321, Ile317, and Met220. We postulated that functionalization of the B-ring *meta* to the ether linkage (Schemes 2 and 3) on **10** would provide an optimal trajectory for accessing this amphiphilic pocket. To the best of our knowledge, few PPAR α agonists exploit this pocket and little SAR exists regarding the effect of occupying this domain on the level of agonism and/or isoform selectivity.

To investigate the possible impact of occupying the amphiphilic pocket, we synthesized two additional derivatives, **26** and **28** (Scheme 3). Briefly, commercially available 2,4-dihydroxybenzaldehyde was treated with 4-methoxybenzaldehyde in the presence of potassium carbonate in acetone to produce the di-*p*-methoxybenzyl (PMB) functionalized resorcinol **25**. This intermediate was coupled to either 3-aminobenzoic acid or **16** followed by reduction of the resulting imine to provide analog **26** and the methyl ester **27**, respectively. Following saponification of **27**, the desired derivative **28** was obtained in 75% yield. Incorporation of the 4-methoxybenzyl motif as the “third-arm” was rather arbitrary at this point and was selected on belief that it 1) would be compatible with the predicted binding environment and 2) could be easily synthesized through dialkylation of an aldehyde already in our chemical inventory.

Derivatives **26** and **28** were evaluated for hPPAR α agonistic activity and selectivity in the luciferase cell-lines. Analysis of the data suggests that regarding the benzoic acid derivatives (compare **10** and **26**), the additional 4-methoxybenzyl substituent does not affect potency and maintains the selectivity, at least within the range of doses evaluated. For derivatives containing the fibrate “head-group” (compare **22** and **28**), however, the addition of the third substituent on the B-ring resulted in a 10-fold improvement in potency, but the *pan*-agonist profile was maintained. Both **26** and **28** were docked using our previously generated model and as can be seen in Fig. 5C the additional 4-methoxybenzyl group is, indeed, predicted to extend into the amphiphilic pocket. Experimental validation is necessary to confirm the binding mode predicted by *in silico* methods, but thus far the SAR data seem to support the models. Studies are ongoing to optimize each of the



Scheme 3. Synthesis of derivatives **26** and **27**. Reagents and conditions: (a) 4-methoxybenzyl bromide, K₂CO₃, Acetone; (b) 3-aminobenzoic acid or **16**, toluene, 155 °C, 2 h; sodium triacetoxyborohydride, AcOH, THF, 0 °C to 25 °C, 12 h; (c) LiOH-H₂O, THF/MeOH/H₂O, 12 h.

three substituents on the B-ring and results will be reported in due course.

In conclusion, we have leveraged *in silico* methods to provide structure-guided insight towards the evolution of a new PPAR α agonistic chemotype. The results confirm our hypothesis that transposition of the carboxylic acid and deconstruction of the rigid quinoline core of Y-0452 provides a more synthetically tractable class of analogs that exhibit promising PPAR α agonism levels and selectivity over other isoforms. Two classes of PPAR agonists have emerged from the initial SAR studies; benzoic acid derivatives that exhibit >20-fold selectivity for PPAR α and a second class that contains the classical fibrate head-group and exhibits *pan*-PPAR agonism. The preliminary results presented suggest that a relatively unexploited amphiphilic pocket provides a promising avenue to interrogate in future SAR studies. Co-crystallization studies are underway to provide more detailed insight into the specific ligand-protein interactions driving PPAR α potency and selectivity within this 4-benzyloxy-benzylamino chemotype.

Acknowledgments

Research reported in this publication was supported by the National Eye Institute of the National Institutes of Health under award number R21EY028279 (A.S.D.). The content is solely the responsibility of the authors and does not necessarily represent the official views of the National Institutes of Health.

A. Supplementary data

Supplementary data associated with this article can be found, in the online version, at <https://doi.org/10.1016/j.bmcl.2018.03.010>.

References

1. Cai X, McGinnis JF. *J Diabetes Res*. 2016. Article ID 3789217.
2. Cheung N, Wong IY, Wong TY. *Diabetes Care*. 2014;37:900.
3. Simo R, Hernandez C. *Prog Retin Eye Res*. 2015;48:160.
4. Lois N, McCarter RV, O'Neill C, Medina RJ, Stitt AW. *Front. Endocrinol.* 2014;5. Article 44.
5. Berger J, Moller D. *Annu. Rev. Med.* 2002;53:409.
6. Feige JN, Gelman L, Michalik L, Desvergne B, Wahli W. *Prog Lipid Res*. 2006;45:120.
7. Michalik L, Wahli W. *Curr Opin Biotechnol*. 1999;10:564.
8. Issemann I, Green S. *Nature*. 1990;347:645.
9. Willson TM, Brown PJ, Sternbach DD, Henke BR. *J Med Chem*. 2000;43:527.
10. Pirat C, Farce A, Lebegue N, et al. *J Med Chem*. 2012;55:4027.
11. Fruchart JC. *Cardiovasc Diabetol*. 2013;12:82.
12. Chen Y, Hu Y, Lin M, et al. *Diabetes*. 2013;62:261.
13. Hu Y, Chen Y, Ding L, et al. *Proc Natl Acad Sci USA*. 2013;110:15401.
14. Ginsberg HN, Elam MB, Lovato LC, et al. *N Engl J Med*. 2010;362:1563.
15. Keech AC, Mitchell P, Summanen PA, et al. *Lancet*. 2007;370:1687.
16. Noonan JE, Jenkins AJ, Ma JX, Keech AC, Wang JJ, Lamoureux EL. *Diabetes*. 2013;62:3968.
17. Gross B, Staels B. *Best Pract Res Clin Endocrinol Metab*. 2007;21:687.
18. Li J, Kennedy LJ, Shi Y, et al. *J Med Chem*. 2010;53:2854.
19. Nentwich MM, Ulbig MW. *World J. Diabetes*. 2015;6:489.
20. Nissen SE, Nicholls SJ, Wolksi K, et al. *J Am Med Assoc*. 2007;297:1362.
21. Wong TY, Simo R, Mitchell P. *Am J Ophthalmol*. 2012;154:6.
22. Cheng R, Ding L, He X, Takahashi Y, Ma JX. *Diabetes*. 2016;3730.
23. Deng G, Moran EP, Cheng R, et al. *Invest Ophthalmol Vis Sci*. 2017;58:5030.
24. Moran E, Ding L, Wang Z, et al. *Invest Ophthalmol Vis Sci*. 2014;55:4568.
25. Xu HE, Lambert MH, Montana VG, et al. *Proc Natl Acad Sci USA*. 2001;98:13919.
26. Bernardes A, Souza PCT, Muniz JRC, et al. *J Mol Biol*. 2013;425:2878.
27. Capelli D, Cerchia C, Montanari R, et al. *Sci Rep*. 2016;6:34792.
28. Gangwal RP, Damre MV, Das NR, Sharma SS, Sangamwar AT. *Bioorg Med Chem Lett*. 2015;25:270.
29. Mizuno CS, Ma G, Khan S, Patny A, Avery MA, Rimando AM. *Bioorg Med Chem*. 2008;16:3800.
30. Nomura M, Tanase T, Ide T, et al. *J Med Chem*. 2003;46:3581.
31. Sierra ML, Beneton V, Boullay AB, et al. *J Med Chem*. 2007;50:685.
32. McMullen PD, Bhattacharya S, Woods CG, et al. *Chem Biol Interact*. 2014;209:14.